Conformational Effects on the Electron-Transfer Efficiency in Peptide Foldamers Based on α,α-Disubstituted Glycyl Residues

by **Emanuela Gatto**[a]), **Alessandro Porchetta**[a]), **Lorenzo Stella**[a]), **Ivan Guryanov**[b]), **Fernando Formaggio**[b]), **Claudio Toniolo**[b]), **Bernard Kaptein**[c]), **Quirinus B. Broxterman**[c]), and **Mariano Venanzi***[a])

[a]) Department of Chemical Sciences and Technologies, University of Rome 'Tor Vergata', I-00133 Rome (e-mail: venanzi@uniroma2.it)

[b]) Institute of Biomolecular Chemistry, Padova Unit, CNR, Department of Chemistry, University of Padova, I-35131 Padova

[c]) DSM Pharmaceutical Products, Advanced Synthesis, Catalysis and Development, NL-MD 6160 Geleen

Peptide foldamers based on α,α-disubstituted glycyl residues were synthesized and chemically characterized to investigate the effects of the electric field generated by a 3_{10}-helix on the rate of intramolecular photoinduced electron-transfer reactions. To this end, two new octapeptides having identical sequences were suitably side-chain functionalized with the same electron-transfer donor–acceptor pair, but inverting the position of the pair along the main chain. The electron-transfer rate constants, measured by time-resolved spectroscopy techniques (nanosecond transient absorption and time-resolved fluorescence), indicated that, in the case of the 3_{10}-helix, the electrostatic effect is significant, but smaller than that obtained for α-helical peptides. This finding can be likely ascribed to the distortion of the H-bond network with respect to the helical axis taking place in the former secondary structure. Overall, these results could have implications on electron-transfer phenomena in model and biomembranes facilitated by peptaibiotics.

Introduction. – In 1966, the isolation from fungal sources of peptides containing Aib (*Fig. 1*), later called peptaibiotics, started an active research effort devoted to the characterization of the bioactivity properties of these molecules, such as their antibiotic action and membrane-perturbing activity [1][2]. However, another fundamental research field initiated by this discovery is concerned with the stereochemical consequences of introducing α,α-disubstituted glycyl residues (such as Aib or (αMe)Nva; *Fig. 1*) into peptide chains. Over the last 30 years, the research efforts of several groups employing many different experimental and theoretical methods have clearly established their strong helix-forming properties. In particular, a high content of Aib residues in a short peptide chain favors the 3_{10}-helix [3], *i.e.*, a regular conformation with approximately three residues per turn and an $i \leftarrow i+3$ intramolecular H-bonding pattern, while longer Aib-containing peptides attain the α-helical conformation (3.6 residues per turn and $i \leftarrow i+4$ H-bonds) [4–10]. L-(αMe)Nva, a chiral α,α-disubstituted glycine, shows a pronounced bias toward the right-handed 3_{10}-helix [8].

As a consequence, peptides comprising α,α-disubstituted glycyl residues are currently used as rigid scaffolds for the specific positioning of electro- or photochemical

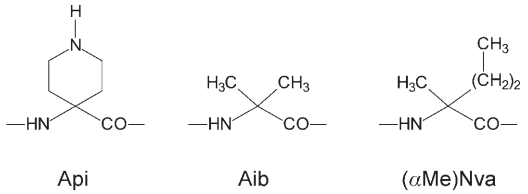

Fig. 1. *Molecular formulae of the α,α-disubstituted glycines Api, Aib, and (αMe)Nva*

moieties at a well-defined distance [11]. In particular, our group has extensively employed these systems in studies of photoinduced electron or energy transfer [12]. In the present study, we took advantage of Aib- and (α-Me)Nva-based oligopeptide 3_{10}-helices to assess the role of the electrical dipole generated by a helical peptide chain in modulating electron-transfer processes, an issue already addressed by *Galoppini* and *Fox* [13][14] for α-helical peptides. A comparison between the different influences of α- and 3_{10}-helices on the efficiency of photoinduced electron-transfer processes has allowed an evaluation of the role of peptide conformation and H-bonding pattern in these phenomena.

The dipole of a peptide bond is *ca.* 3.5 D. In the α-helix, these dipoles are aligned along the helix axis, producing an effective positive charge at the N-end and an effective negative charge at the C-end [13][14]. Polarization effects due to H-bonding increase the dipole moment per residue to 5.2 D [15]. This strong electric field plays an important role in the structure and function of proteins. In contrast, in a 3_{10}-helix the H-bonds are not perfectly aligned with respect to the helical axis, and hence the resulting total molecular dipole is smaller than in the α-helix (4.6 D per residue) [15][16]. Furthermore, the different H-bonding patterns in the two helical conformations could influence the electronic coupling between donor and acceptor moieties linked to the peptide chain [15].

To analyze the effect of the electric field generated by a 3_{10}-helix on intramolecular electron-transfer processes, three terminally blocked octapeptides were synthesized, comprising Aib, (αMe)Nva, and Api, the last α,α-disubstituted glycine being characterized by a $C(\alpha)_i$–$C(\alpha)_i$ cyclization (*Fig. 1*) [17][18].

The primary structures of the peptides investigated are as follows:

P2: Z-Aib-Api(Pyr)-L-(αMe)Nva-Aib-L-(αMe)Nva-(αMe)Nva-Aib-Api-(Boc)-NH^{t}Bu

P2A8: Z-Aib-Api(Pyr)-L-(αMe)Nva-Aib-L-(αMe)Nva-(αMe)Nva-Aib-Api-(Azu)-NH^{t}Bu

A2P8: Z-Aib-Api(Azu)-L-(αMe)Nva-Aib-L-(αMe)Nva-(αMe)Nva-Aib-Api-(Pyr)-NH^{t}Bu

(for the formulae of Api(Azu) and Api(Pyr), see *Fig. 2*). The notations **P2**, **P2A8**, and **A2P8** emphasize the different positions of the chromophoric moieties along the main chain.

The oligopeptides **P2A8** and **A2P8**, having pendant electron donor (D; pyrene) and acceptor (A; azulene) chromophores, differ only in the relative positions of the donor–acceptor (D–A) pair along the helix dipole [13][14]. Thus, the photoinduced electron-

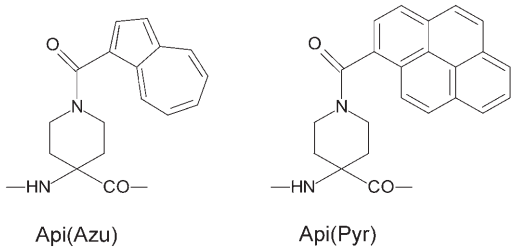

Fig. 2. *Molecular formulae of the Api(Azu) and the Api(Pyr) residues*

transfer process between D and A should be affected by the orientation of the electric field determined by the helix dipole. Steady-state and time-resolved fluorescence experiments, together with laser-induced spectroscopy on transient species, were performed to investigate this phenomenon.

Results. – *Peptide Synthesis and Characterization.* For the large-scale production of the enantiomerically pure L-(αMe)Nva, we exploited an economically attractive and generally applicable chemo-enzymatic synthesis developed by *DSM Pharmaceutical Products* a few years ago [19].

For the preparation of the terminally blocked octapeptide **P2**, we used the segment-condensation approach in solution (*Scheme 1*). Tripeptide **3A**-OH was coupled to the *N*-deprotected tripeptide **3B**, and the resulting N-terminal hexapeptide **6AB**, after *C*-deprotection, was reacted with the N^{α}-deprotected dipeptide **2C** (*tert*-butyl)amide to generate the octapeptide **8ABC** (**P2**). The amino acid derivative Z-Api(Pyr)-OH was

Scheme 1. *Segment-Condensation Approach Used for the Synthesis of the Terminally Blocked Octapeptide* **P2**

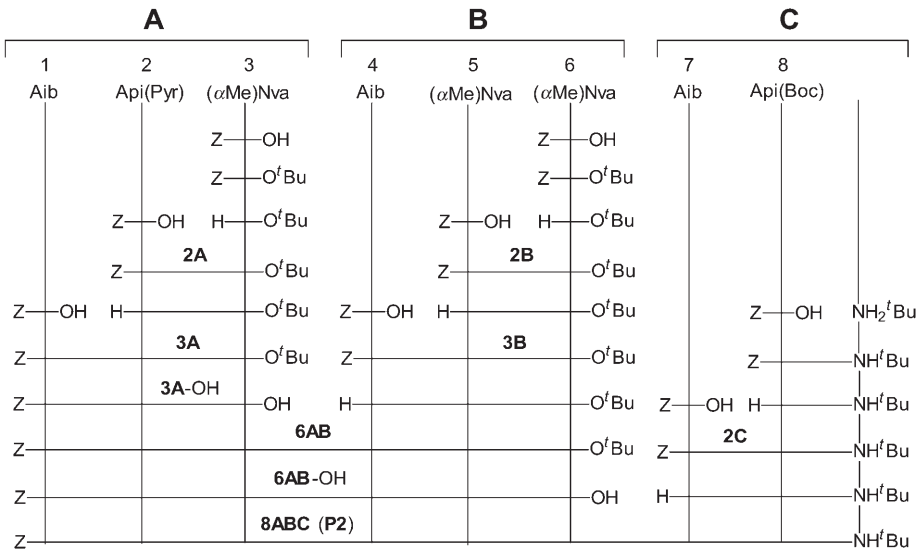

prepared from Z-Api(Boc)-OH [20], which was *C*-protected as Z-Api(Boc)-OBg upon treatment with BrBg [21]. Then, the side-chain Boc group was removed, and the Pyr group was incorporated by use of Pyr-COOH, affording Z-Api(Pyr)-OBg. Finally, OBg *C*-deprotection by alkaline hydrolysis gave Z-Api(Pyr)-OH, which was exploited for the synthesis of dipeptide **2A**. Z-Aib-OH [22] and Z-L-(αMe)Nva-OH [23] are known products. All amide (or peptide) bond formations were achieved using 1-[3-(dimethylamino)propyl]-3-ethylcarbodiimide hydrochloride (EDC; in a few cases, in the presence of the efficient additive 7-aza-1-hydroxy-1,2,3-triazole (HOAt) [24]) in CH_2Cl_2 solution. Removals of the ^{t}BuO ester and Boc urethane functions were accomplished by mild acidolyses with a 1:1 CH_2Cl_2/TFA mixture. The Z N^{α}-protection was removed by catalytic hydrogenation in MeOH solution.

The octapeptide **P2A8** (≡**8′ABC**) was prepared by deprotecting under acidic conditions the side chain of Api(Boc) in the octapeptide **P2** (≡**8ABC**) and coupling the resulting compound with Azu-COOH/EDC/HOAt.

Since, in our experience with the model dipeptide Z-Api(Azu)-L-(αMe)Nva-O^{t}Bu, the Azu group does not survive a catalytic hydrogenolysis treatment, we partly modified *Scheme 1* for the synthesis of octapeptide **A2P8** (*Scheme 2*). We first prepared the C-terminal pentapeptide **5B″C″** by condensing the tripeptide segment **3B″**-OH with the *N*-deprotected dipeptide **2C″**. The octapeptide **8″** was synthesized

Scheme 2. *Partial Segment-Condensation Approach Used for the Synthesis of the Terminally Blocked Octapeptide* **A2P8**

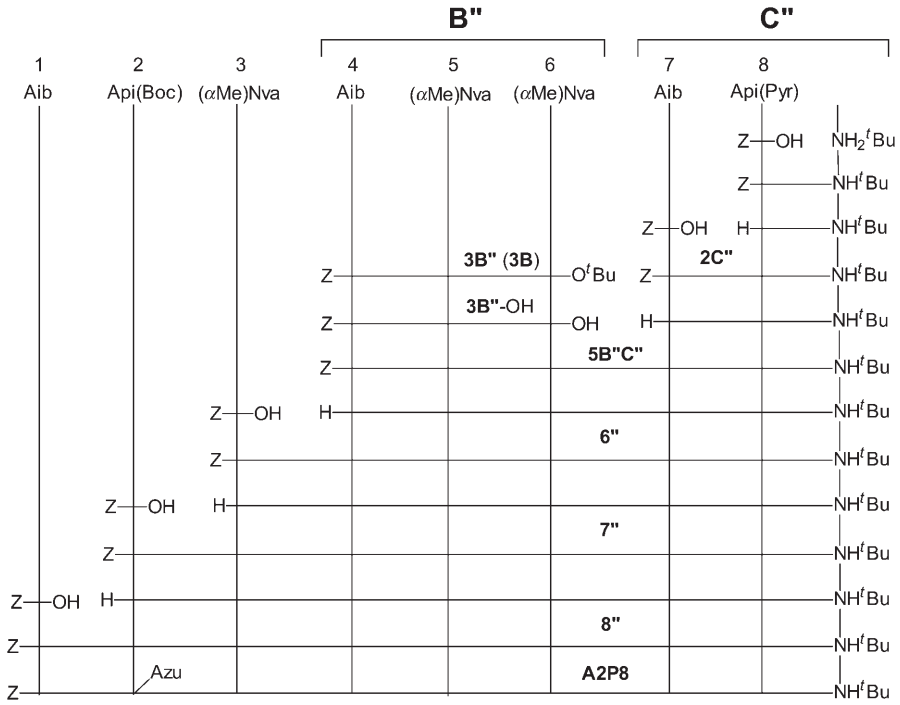

from **5B″C″** by three successive steps using Z-L-(αMe)Nva-OH, Z-Api(Boc)-OH, and Z-Aib-OH. In the last step, the side chain of Api(Boc) in the octapeptide **8″** was deprotected, and the resulting octapeptide was reacted with Azu-COOH/EDC/HOAt to afford the desired octapeptide **A2P8**.

The various peptides and their synthetic intermediates were characterized by melting-point determination, optical rotatory power, TLC in three different eluant systems, and solid-state IR absorption (*Table 1*). All amino acid derivatives and peptides were also checked by ^{1}H-NMR and the longest peptides by ESI-TOF mass spectrometry as well (results not shown).

UV Absorption. *Fig. 3* shows the UV absorption spectra of the peptides **P2A8** and **A2P8**, and the reference compounds, containing only the pyrene (peptide **P2**) or the azulene [Z-Api(Azu)-OH] chromophore.

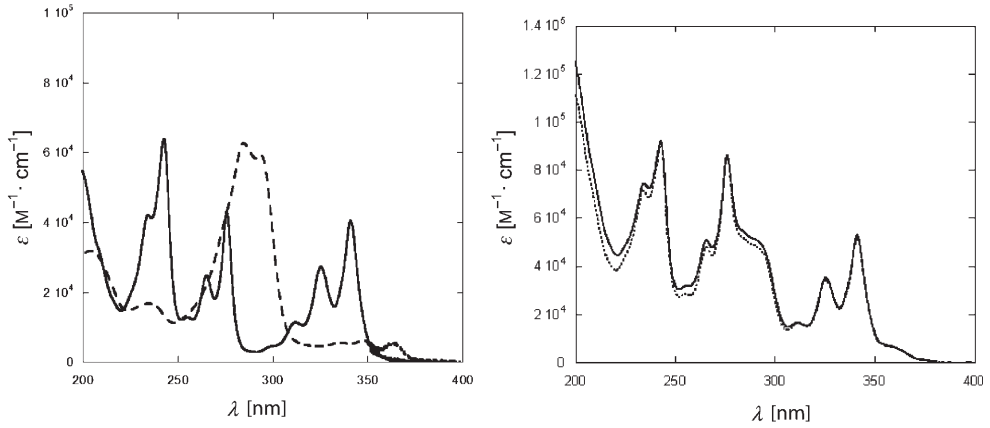

Fig. 3. *Absorption spectra of* **P2** (solid line) *and Z-Api(Azu)-OH* (dashed line) (left), *and of* **P2A8** (dotted line) *and* **A2P8** (solid line) (right) *in MeCN solution*

The spectra of the peptides **P2A8** and **A2P8**, very similar to each other, exhibit a combination of the same absorption bands of the pyrenyl [25] and azulenyl [26–28] components, indicating the absence of any strong ground-state interaction between D and A in both peptides.

Peptide Conformation. CD and IR Absorption. To determine the conformational preferences of the peptides investigated, we have performed CD and IR absorption experiments. The CD spectra of **P2**, **P2A8**, and **A2P8** in MeCN solution, shown in *Fig. 4*, exhibit an intense negative maximum around 202–205 nm, typical of peptides attaining a right-handed 3_{10}-helical conformation [29][30]. In the 230–250-nm range some differences among the three peptides can be noted, probably due to an induced CD resulting from electronic transitions of the aromatic side chains (pyrene and azulene), caused by the nearest-neighbor peptide groups [31][32].

The IR absorption spectra in $CDCl_3$ solution of the peptides **P2** and **P2A8**, and their synthetic precursors Z-Aib-Api(Pyr)-L-(αMe)Nva-O^{t}Bu and Z-Aib-Api(Pyr)-L-(αMe)Nva-Aib-L-(αMe)Nva-L-(αMe)Nva-O^{t}Bu are shown in *Fig. 5*. In the N–H stretching region, two characteristic bands were observed at *ca.* 3430 and 3330 cm^{-1}.

Table 1. *Physical Data and Analytical Properties of the Newly Synthesized Compounds*

Peptide	Yield [%][a])	M.p. [°]	Crystallization solvent[b])	$[\alpha]_D^{20}$ [c])	LC R_f values [d])			IR Absorption [cm^{-1}][e])
					I	*II*	*III*	
Octapeptide **P2** (*Scheme 1*):								
Z-Api(Boc)-OBg	73	156–158	AcOEt/PE	–	0.80	0.95	0.35	3433, 3316, 1753, 1693, 1545
Z-Api(Pyr)-OBg	68	136–138	AcOEt/PE	–	0.65	0.95	0.30	3423, 1743, 1705, 1648, 1538
Z-Api(Pyr)-OH	75	227–229	MeOH/Et_2O	–	0.20	0.95	0.10	3407, 1741, 1687, 1531
Z-Api(Boc)-NH^{t}Bu	70	143–145	AcOEt/PE	–	0.70	0.95	0.45	3426, 1717, 1694, 1651, 1535
2A	35	150–152	AcOEt/PE	−2.6	0.65	0.95	0.45	3430, 3392, 3315, 1726, 1668, 1630, 1525
3A	55	233–235	AcOEt/PE	−6.4	0.65	0.95	0.30	3402, 3352, 1716, 1678, 1618, 1510
3A-OH	90	151–153	MeOH/Et_2O	1.0	0.15	0.95	0.05	3411, 1705, 1678, 1618, 1511
Z-L-(αMe)Nva-O^{t}Bu	87	oil	AcOEt/PE	−4.1[f])	0.95	0.95	0.85	3418, 3361, 1719
2B	71	71–73	AcOEt/PE	−0.9	0.95	0.95	0.40	3391, 3332, 1726, 1669
3B	66	109–111	AcOEt/PE	−7.0	0.65	0.95	0.45	3439, 3339, 1737, 1708, 1648, 1535
2C	77	194–196	AcOEt/PE	–	0.65	0.95	0.30	3393, 3302, 1719, 1693, 1674, 1531
6AB	75	159–161	AcOEt/PE	−11.9	0.80	0.95	0.30	3420, 3333, 1727, 1701, 1665, 1528
8ABC (**P2**)	70	212–214	AcOEt/PE	−1.2[g])	0.55	0.95	0.30	3426, 3319, 1660, 1530
Octapeptide **P2A8**:								
8′ABC (**P2A8**)	47	210–212	AcOEt/PE	−15.8[f])	0.50	0.95	0.15	3426, 3321, 1661, 1532
Octapeptide **A2P8** (*Scheme 2*):								
Z-Api(Pyr)-NH^{t}Bu	63	195–197	AcOEt/PE	–	0.60	0.95	0.40	3425, 3390, 3314, 1723, 1650, 1627, 1527
2C″	37	211–213	AcOEt/PE	–	0.65	0.95	0.30	3416, 3388, 3304, 1710, 1670, 1625, 1530
5B″C″	82	139–141	AcOEt/PE	−9.4	0.80	0.95	0.40	3425, 3326, 1704, 1664, 1617, 1530
6″	30	145–147	AcOEt/PE	−17.9	0.80	0.95	0.25	3319, 1661, 1530
7″	78	155–157	AcOEt/PE	7.6	0.80	0.95	0.25	3314, 1659, 1533
8″	60	160–161	AcOEt/PE	2.8	0.60	0.95	0.35	3305, 1657, 1532
A2P8	60	163–165	AcOEt/PE	−24.5[h])	0.55	0.95	0.15	3307, 1657, 1531
Model dipeptide:								
Z-Api(Azu)-OBg	75	164–166	AcOEt/PE	–	0.65	0.95	0.35	3420, 1749, 1675, 1533
Z-Api(Azu)-OH	75	105–107	MeOH/Et_2O	–	0.15	0.95	0.10	3405, 3336, 1721, 1533
Z-Api(Azu)-L-(αMe)Nva-O^{t}Bu	45	78–80	AcOEt/PE	−8.7[f])	0.95	0.95	0.40	3396, 3306, 1725, 1672, 1539

[a]) Yields refer to the last step. [b]) PE, petroleum ether. [c]) $c=0.5$, MeOH. [d]) For eluants, see *Exper. Part.* [e]) For the solid-state IR absorption spectra only bands in the 3500–3250 and 1800–1500 cm^{-1} regions are reported. [f]) $[\alpha]_{436}^{20}$, $c=0.3$, MeOH. [g]) $c=0.3$, MeOH. [h]) $[\alpha]_{436}^{20}$, $c=0.2$, MeOH.

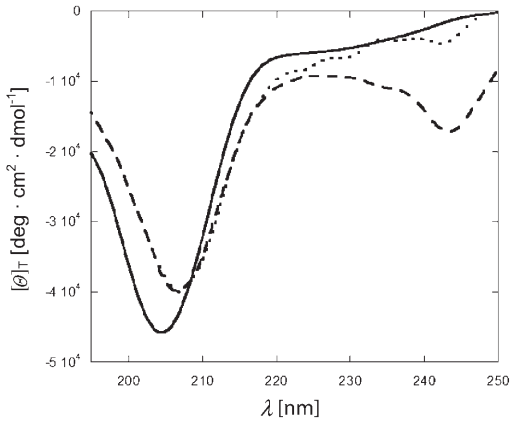

Fig. 4. *Far-UV-CD spectra of the* **P2** (solid line), **P2A8** (dotted line), *and* **A2P8** (dashed line) *in MeCN solution.* Peptide concentration: 1×10^{-4} M.

The first band is associated with NH groups not involved in H-bond interactions, while the second band is typical of H-bonded NH groups [33][34]. The relative area of the latter transition increases with the length of the backbone, thereby denoting a greater number of residues participating in the H-bond network, while the former transition shows no intensity change with peptide chain elongation [35][36]. This finding suggests that only the N-terminal NH groups are not involved in intramolecular H-bonds, as expected for a peptide helical structure. No significant changes were observed in the IR absorption spectra when varying the peptide concentration between 10^{-4} and 10^{-2} M (spectra not shown), ruling out self-association *via* intermolecular H-bonds.

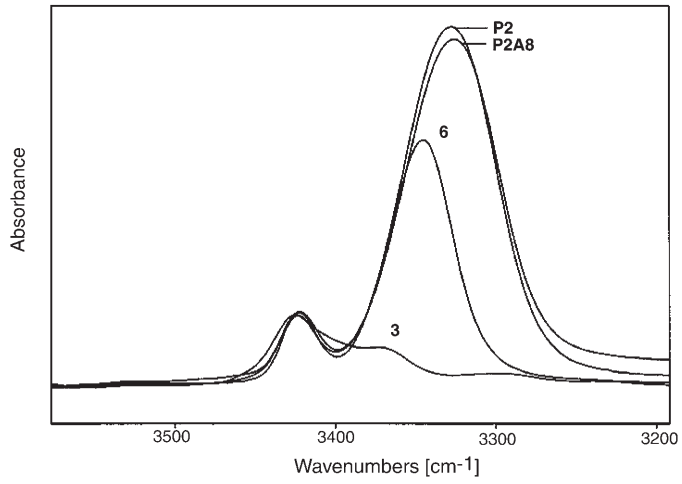

Fig. 5. *IR Absorption spectra of the Z-Aib-Api(Pyr)-*L*-(αMe)Nva-O*^{t}*Bu* (**3**), *Z-Aib-Api(Pyr)-*L*-(αMe)Nva-Aib-*L*-(αMe)Nva-*L*-(αMe)Nva-O*^{t}*Bu* (**6**), **P2**, *and* **P2A8** *in* $CDCl_3$ *solution in the 3500–3200-*cm^{-1} *region.* Peptide concentration: 1×10^{-3} M.

The present IR absorption results support the conclusion that intramolecularly H-bonded structures are largely populated by these octapeptides in solution and, combined with the CD data, suggest that the compounds investigated are folded in right-handed 3_{10}-helical conformations.

Steady-State and Time-Resolved Fluorescence. We next examined the excited-state behavior of the pyrene-azulene octapeptides. Steady-state fluorescence experiments in MeCN solution show a substantial quenching of the pyrene emission by azulene for both **A2P8** and **P2A8**, as illustrated in *Fig. 6* (λ_{ex} 341 nm). The fluorescence quantum yields (ϕ) are given in *Table 2*. Interestingly, the quantum yield of **P2A8** is greater than that of **A2P8**, indicating a more efficient quenching in the latter peptide. It should be noted that the azulene emission is negligible, and the fluorescence quantum yield of the pyrenyl peptide **P2** ($\phi = 0.063$) is by one order of magnitude lower than that of pyrene ($\phi = 0.72$) [37], probably because of the carbonyl derivatization.

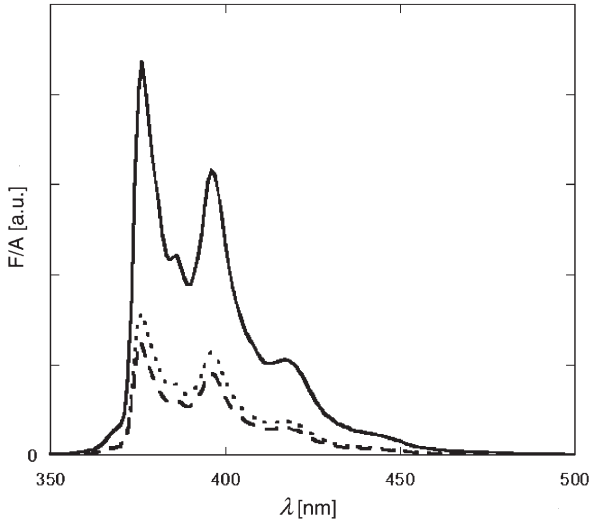

Fig. 6. *Steady-state fluorescence spectra of* **P2** (solid line), **P2A8** (dotted line), *and* **A2P8** (dashed line) *in MeCN solution* (λ_{ex} 341 nm)

Table 2. *Quantum Yields* (ϕ), *Average Lifetimes* ($\langle\tau\rangle$), *and Dynamic Quenching Rate Constants* (k_q) *of the Pyrene-Azulene Octapeptides in MeCN Solution*[a])

Peptide	ϕ	$\langle\tau\rangle$	k_q [10^{-8} s^{-1}]
P2	0.063	11.7	
P2A8	0.022	6.4	0.7
A2P8	0.017	4.8	1.2

[a]) λ_{ex} 341 nm.

Time-resolved fluorescence experiments are reported in *Fig. 7*. All time decays can be reproduced by a multiexponential fitting function (*Table 3*), suggesting the existence of several ground-state conformers. In agreement with the steady-state

results, the average fluorescence lifetime $\langle\tau\rangle$ of the peptide **P2** (11.7 ns; *Table 2*) is much shorter than that of the pyrene molecule in solution (200 ns), and both **A2P8** and **P2A8** are significantly quenched with respect to the reference compound **P2**. This quenching can be explained in terms of intramolecular photoinduced electron transfer, but resonance-energy transfer is very likely taking place as well, since the absorption spectrum of the azulene chromophore partially overlaps with the emission spectrum of the pyrene moiety [38].

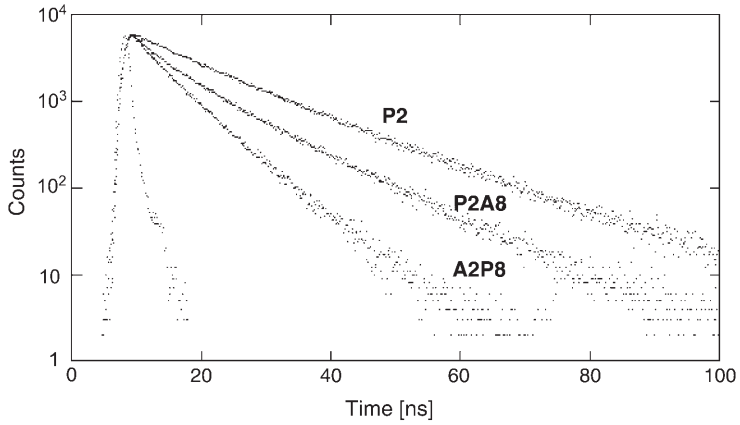

Fig. 7. *Fluorescence decay curves of* **P2**, **P2A8**, *and* **A2P8** (λ_{ex} 341, λ_{em} 410 nm). The lamp profile is also shown.

Table 3. *Time Decay Parameters of Excited Pyrene in the Pyrene-Azulene Octapeptides in MeCN and DMSO Solutions*[a])

Solvent	Peptide	α_1	τ_1 [ns]	α_2	τ_2 [ns]	α_3	τ_3 [ns]	χ^2
MeCN	**P2**	0.14	1.2	0.37	9.4	0.49	16.4	1.10
	P2A8	0.32	1.3	0.34	5.5	0.34	12.2	1.00
	A2P8	0.4	2.3	0.59	6.6			1.03
DMSO	**P2**	0.34	2.7	0.65	5.9	0.01	22.4	1.07
	P2A8	0.33	1.2	0.56	4.3	0.11	7.6	1.07
	A2P8	0.31	1.3	0.66	3.8	0.02	7.8	1.00

[a]) λ_{ex} 341 nm, λ_{em} 410 nm. The uncertainty in lifetimes is *ca.* 5% for the long components and *ca.* 10% for the short components. The uncertainty in the pre-exponents is *ca.* 10%.

The total quenching rate constants (*Table 2*) were calculated from the average lifetimes of the pyrenyl group in the peptides ($\langle\tau\rangle$) and in the reference compound **P2** ($\langle\tau_0\rangle$), as given by:

$$\langle k_{ET}\rangle = \frac{1}{\langle\tau\rangle} - \frac{1}{\langle\tau_0\rangle}$$

In agreement with the steady-state results, the quenching rate constant of **A2P8** is greater than that of **P2A8**.

Peptide destructuration would provide a useful test for the influence of the helical dipole on the measured decay rates, as the net dipole of a fully unordered peptide is zero [12]. Generally, DMSO is used as a structure-disrupting solvent, since the sulfoxide group promotes the formation of S=O···H–N intermolecular H-bonding, competing effectively with the intramolecular C=O···H–N H-bonds present in the helix [39]. For this reason, time-resolved fluorescence experiments were also performed in DMSO. Also in this case, time decays are described by multiexponential functions, as reported in *Table 3*. Average lifetimes and quenching rate constants are listed in *Table 4:* no significant differences are observed in the quenching rates with respect to those obtained in MeCN solution, suggesting that DMSO is not able to unfold the extremely stable 3_{10}-helix based on eight constituent α,α-disubstituted glycyl residues. Unfortunately, CD experiments to confirm this conclusion cannot be performed in this latter solvent, because of its strong absorption in the peptide spectral region (195–250 nm).

Table 4. *Average Lifetimes* ($\langle\tau\rangle$) *and Dynamic Quenching Rate Constants* (k_q) *of the Pyrene-Azulene Octapeptides in DMSO Solution*[a])

Peptide	$\langle\tau\rangle$	k_q ($\times 10^{-8}$) [s^{-1}]
P2	5.0	
P2A8	3.6	0.8
A2P8	3.1	1.2

[a]) λ_{ex} 341 nm.

Transient Absorption. Transient-absorption experiments with nanosecond resolution were carried out to further characterize the electron-transfer process between the azulene and pyrene groups in the excited state, and to determine the charge recombination rate constants for the back-electron-transfer reactions.

All transient absorption decays could be described satisfactorily with a double exponential decay. The two components could be assigned to the pyrene radical cation and pyrene triplet–triplet absorptions, based on the corresponding decay-associated spectra (*Fig. 8*), which exhibit the absorption maxima typical of these species (450 and 420 nm, resp.) [40–44]. This spectral assignment was further confirmed by experiments performed in the presence of oxygen (data not shown), which suggested a much lower triplet–triplet contribution, due to efficient quenching of this species. The presence of signals of radical species also in the octapeptide **P2**, which lacks the electron acceptor azulene, indicates the occurrence of an electron-transfer process from pyrene to the peptide backbone, as previously reported [45–49]. Transient absorption measurements in the same wavelength region on the simple derivative Z-Api(Azu)-OH did not reveal any specific feature, probably because of the very small singlet to triplet intersystem-crossing efficiency in the azulene chromophore [50][51]. Furthermore, no absorption features ascribable to the pyrene radical anion (λ_{max} 490 nm [42][43][52]) were observed, a finding that rules out an electron-transfer process from azulene to pyrene. The rate constants associated to the triplet state and the cation radical decay, and the relative transient absorptions derived from the global analysis of the time-dependent

spectra, are reported in *Table 5*. These data conclusively confirm the presence of an effect of the electrical field induced by the peptide helix dipole on the back-electron-transfer process, since the rate of radical cation decay is 1.5 times higher in **P2A8** than in **A2P8**.

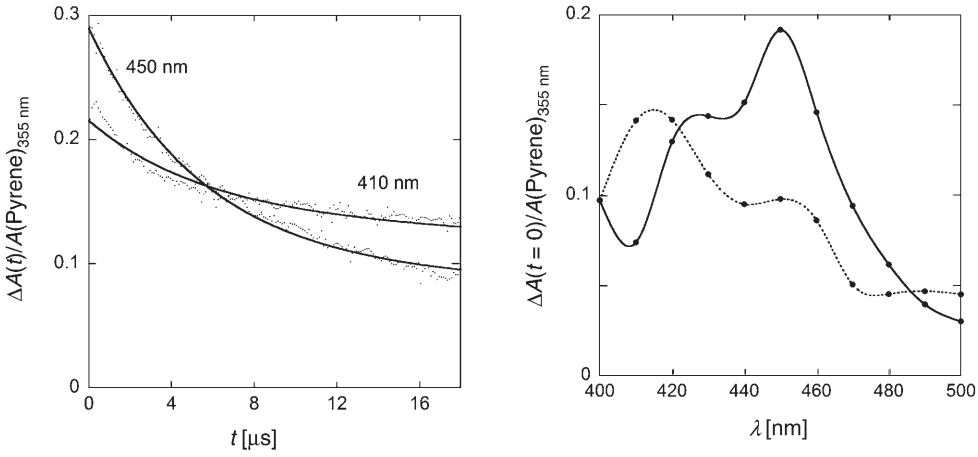

Fig. 8. *Transient absorption experiments for the reference peptide* **P2**. *Left:* decay curves at two representative wavelengths. Curves resulting from the global double exponential fit are shown as solid lines. *Right:* transient absorption decay associated spectra (at $t=0$), derived from the global fit. *Solid line:* radical cation; *dotted line:* triplet state. All transient absorption values are normalized by sample absorbance at the laser excitation wavelength (355 nm).

Table 5. *Decay Parameters from a Global Analysis of Transient Absorption Experiments on the Pyrene-Azulene Octapeptides in MeCN Solution*

Peptide	$\Delta A_{tot}/A$ [a])	k_T [b]) ($\times 10^{-4}$) [s^{-1}]	$\Delta A_T/A$ [c])	α_T [d])	k_c [e]) ($\times 10^{-5}$) [s^{-1}]	$\Delta A_C/A$ [f])	α_C [g])
P2	0.289	0.6 ± 0.1	0.098	0.34	1.82 ± 0.05	0.191	0.66
P2A8	0.095	2.7 ± 0.2	0.021	0.26	6.9 ± 0.2	0.059	0.74
A2P8	0.100	4.9 ± 0.5	0.026	0.26	5.0 ± 0.2	0.074	0.74

[a]) Total differential absorption at $t=0$, λ 450 nm, normalized for the absorption of the pyrene chromophore at 355 nm. [b]) Triplet decay rate constant. [c]) Differential triplet absorption at $t=0$, λ 450 nm, normalized for the absorption of the pyrene chromophore at 355 nm. [d]) Fractional contribution of the triplet state to the transient absorption intensity at 450 nm. [e]) Rate constant of the radical cation decay. [f]) Differential radical cation absorption at $t=0$, $\lambda=450$ nm, normalized for the absorption of the pyrene chromophore at 355 nm. [g]) Fractional contribution of the radical cation to the transient absorption intensity at 450 nm.

Discussion. – This study analyzes the effects of the electrostatic field generated by a 3_{10}-helical peptide on the rate of intramolecular photoinduced electron-transfer processes, and how these compare to the effects generated by α-helical peptides [13][14].

The influence of an electrostatic field on electron-transfer rates can be illustrated in terms of the simple semiclassical *Marcus* theory [53][54]. The rate constant of electron transfer (k_{ET}) from a donor to an acceptor at a fixed distance is described by the following equation:

$$k_{ET} = \sqrt{\frac{4\pi^3}{h^2 \lambda k_B T}} H_{DA}^2 \exp\left[-\frac{(\Delta G^0 + \lambda)^2}{4\lambda k_B T}\right]$$

$$H_{DA}^2 = (H_{DA}^0)^2 \exp(-\beta r)$$

where h is *Planck*'s constant, λ the reorganization energy, k_B the *Boltzmann*'s constant, T the absolute temperature, H_{DA}^2 the electronic coupling strength between donor and acceptor, $(H_{DA}^0)^2$ the coupling strength at the closest contact, ΔG^0 the driving force for the electron-transfer reaction, β the tunneling parameter for the medium, and r the edge-to-edge donor–acceptor distance. Any energy effects due to electrostatic interactions between the helical field and the photogenerated $D^{\cdot+}A^{\cdot-}$ couple are included in the ΔG^0 term. Therefore, the electron-transfer rate must depend on the positioning of D and A with respect to the peptide helical dipole. The alignment of the electric field with respect to the direction of the photoinduced electron transfer should induce a faster electron-transfer rate in **A2P8** than in **P2A8**. In contrast, the back-electron-transfer charge-recombination process should be relatively favored in **P2A8**. In principle, the different peptide conformations could influence also the coupling between donor and acceptor, and, therefore, the tunneling parameter β. However, quantum-chemical calculations suggest that this parameter is comparable in the 3_{10}- and α-helices [15].

Fluorescence quenching experiments did show different decay rates for the excited pyrene in the two peptides **A2P8** and **P2A8** (with a ratio of *ca.* 1.7). However, a simple interpretation in terms of electron transfer is not warranted, since different observations indicate that resonance energy-transfer processes from pyrene to azulene cannot be neglected. The *Förster* radius R_0 for pyrene and azulene, *i.e.*, the characteristic distance at which the energy-transfer efficiency is 50%, can be calculated from the emission and absorption spectra of the two fluorophores [38]. The obtained R_0 value of 14.1 Å is larger than the approximate distance of 12 Å between the two moieties, calculated by assuming a translational distance per residue of 2 Å typical of the 3_{10}-helix [3], and considering that the D and A chromophores are separated by six residues in the octapeptides investigated. A direct indication that energy-transfer processes are indeed taking place is provided by the transient absorption experiments. If electron transfer to azulene is the main quenching mechanism of the pyrene excited singlet state, a higher population of the radical cation species would be expected in the peptides **A2P8** and **P2A8** with respect to the reference octapeptide **P2**. In contrast, these peptides exhibited a *reduced* transient absorption (*Table 5*), both for the radical cation and the triplet state, indicating an efficient quenching of the pyrene excited singlet state by a process different from electron transfer.

A better insight in the electron-transfer process can be derived from the transient absorption experiments. The overall transient absorptions of **A2P8** and **P2A8** are

reduced with respect to that of **P2**, because of the more efficient quenching of the pyrene excited singlet state. However, the fraction of the observed signal associated to the radical cation is slightly higher in these peptides than in the reference compound **P2**, showing that a photoinduced electron-transfer process is indeed taking place. The time resolution of our transient absorption setup is limited to processes slower than *ca.* 10 ns by the width of the pump laser pulse. Therefore, our data do not allow a direct observation of the population of the radical cation species produced by the electron-transfer process. In contrast, the back-electron-transfer phenomenon, causing the decay of the radical cation, can be followed easily. The influence of the peptide helix electric field on this process should be reversed from the case of formation of the charge-separated state. Accordingly, the measured rate constants for charge recombination exhibit a ratio **P2A8**/**A2P8** of *ca.* 1.5. In summary, our results indicate that the electric field generated by the peptide helix has a significant effect on the electron-transfer rate for both the photoinduced charge separation process and the back-electron-transfer charge recombination.

It is interesting to relate these findings with those obtained for α-helical peptides, where a ratio of eight between the two electron-transfer rates was observed [13][14]. Even if the two data sets are not strictly comparable, because of differences in the peptide sequence, the present results suggest that the 3_{10}-helix has a lower effect than the α-helix on the intramolecular electron-transfer process. This observation is in agreement with recent experiments performed by electrochemical methods on 3_{10}-helical peptides covalently linked to a gold surface [55], showing that the helix dipole moment affects the electron-transfer rate toward the gold substrate. Also in that case, the effect was lower in 3_{10}-helical than in α-helical peptides. Excluding possible differences between the 3_{10}- and the α-helix in the coupling provided by the peptide bridge for the long-range electron-transfer process, quantified by the tunneling parameter β [15], the observed differences between the two helical conformations are very likely due to the imperfect alignment of the peptide dipoles in the 3_{10}-helix [3], leading to a lower overall electric field.

Conclusions. – Combination of various spectroscopic techniques (UV absorption, CD, IR absorption, nanosecond transient absorption, and steady-state and time-resolved fluorescence) allowed us to determine the effect of the electric field generated by a peptide 3_{10}-helix on the rate of intramolecular electron-transfer reactions. The data obtained indicate that a significant effect of this electrostatic field takes place on the electron-transfer rates for both the photoinduced electron-transfer and the charge-recombination processes. However, this influence is lower than that previously observed for α-helical peptides [13][14], probably because of the imperfect alignment of peptide dipoles in the 3_{10}-helix, leading to a lower overall electrostatic field. These results could also be of relevance to electron-transfer processes across model and biological membranes induced by 3_{10}-/α-helical peptaibiotics.

Experimental Part

General. Abbreviations: Aib, α-Aminoisobutyric acid; (αMe)Nva, $C(\alpha)$-methyl norvaline; Api, 1-aminopiperidine-1-carboxylic acid; Azu, azulen-1-ylcarbonyl; BgO, *N*-benzhydrylglycolamide; Boc,

(*tert*-butoxy)carbonyl; EDC, 1-[3-(dimethylamino)propyl]-3-ethylcarbodiimide hydrochloride; HOAt, 7-aza-1-hydroxy-1,2,3-benzotriazole; NH^{t}Bu, (*tert*-butyl)amino; O^{t}Bu, *tert*-butoxy; PE, petroleum ether; Pyr, pyren-1-ylcarbonyl; TFA, trifluoroacetic acid; Z, (benzyloxy)carbonyl. Anal. TLC: silica gel *F254* (*Merck*); eluant systems: 10% EtOH/$CHCl_3$ (*I*); 20% AcOH, 60% butan-1-ol (*II*); 15% EtOH/toluene (*III*); UV detection (254 nm) for all compounds. Anal. HPLC: *Pharmacia LKB-LCC* chromatograph equipped with a *Uvicord SD* absorbance detector (226 nm); reversed-phase C_{18} *Agilent Zorbax* (5 μm) column (250 × 4.6 mm); eluant systems: 0.05% TFA/H_2O (*A*); 0.05% TFA/10% H_2O/MeCN (*B*); gradient 70 to 90% *B* in 25 min; flow rate: 1 ml/min. M.p.: *Leitz Laborlux 12* apparatus; determination with a temp. raise of 3°/min; uncorrected. $[\alpha]_D$: *Perkin-Elmer 241* polarimeter, 1-dm thermostatted cell. FT-IR Absorption spectra: solid-state IR by the KBr disk technique, with a *Perkin-Elmer 580 B* spectrophotometer equipped with a *Perkin-Elmer 3600* IR data station. ^{1}H-NMR Spectra: in $CDCl_3$ (99.96% D; *Aldrich*) at 400 MHz, *Bruker AM-400* spectrometer; δ in ppm rel. to Me_4Si as internal standard, *J* in Hz. MS: *Perseptive Biosystems Mariner* ESI-TOF. Physical data and anal. properties for the newly prepared peptides are listed in *Table 1*.

Electronic Absorption. All the electronic absorption experiments were carried out at r.t. on solns. in quartz cuvettes (optical pathlength 1 cm) with a *Cary 100* scan spectrophotometer. The concentrations of the solns. were typically 10^{-5}–10^{-4} M. Extinction coefficient values were determined by using the *Lambert–Beer* law. The exper. error on the sample concentrations was estimated to be ±10%.

Circular Dichroism. CD Spectra were recorded on a *Jasco J-600* dicrograph with a 0.1-cm pathlength quartz cell. Concentrations of peptide solns. were 10^{-4} M.

IR Absorption. IR Absorption measurements in soln. were performed on a *Perkin-Elmer* model *1720 X* FTIR spectrophotometer, N_2-flushed, equipped with a sample-shuttle device, at 2-cm^{-1} nominal resolution, averaging 100 scans. Solvent (baseline) spectra were obtained under the same conditions. Cells with pathlengths of 0.1, 1, and 10 mm (with CaF_2 windows) were used.

Fluorescence. Steady-state fluorescence spectra were recorded on a *SPEX Fluoromax* spectrofluorimeter, operating in the single photon counting mode. All experiments were performed using a thermostat at 298 K. Solns. were in quartz cuvettes (absorbance at excitation wavelength ≈0.03; optical pathlength 1 cm). Quantum yields were determined by using a fluorescent standard, the quantum yield of which was known, and the emission spectral properties of which closely matched those of the compound under investigation. The quantum yield of the sample is then operationally defined as:

$$\phi_s = \phi_r\,(A_r/A_s)\,(F_s/F_r)(n_s/n_r)^2$$

where ϕ is the quantum yield, *A* is the absorbance at the excitation wavelength, *F* is the integrated emission area across the band, *n* the refractive index of the solvent, and the subscripts s and r refer to the sample and the reference, resp. The reference used was anthracene in EtOH ($\phi_0 = 0.27 \pm 0.03$). The exper. errors were ±15%. Fluorescence decay was measured with a *CD900* single photon counting apparatus from *Edinburgh Analytical Instruments*. The excitation source was a gas discharge lamp (model *nF 900*) filled with ultrapure H_2 for excitation in the UV range. Under the exper. conditions (300 mm Hg gas pressure, 40 kHz repetition rate) used, the full-width half-maximum of the excitation profile was 1.2 ns. Decay curves were fitted by a non-linear least-squares analysis to exponential functions by an iterative deconvolution method. All experiments were carried out in quartz cells using solns. previously bubbled for 20 min with ultrapure N_2.

Transient Absorption. Nanosecond transient absorption experiments were performed with an *LKS 60* apparatus (*Applied Photophysics*) using a *Brilliant B Nd YAG Q*-switched laser (*Quantel*) equipped with a third harmonic generator module to obtain a 355-nm excitation light with a pulse duration of 4 ns (full-width half-maximum) and an energy of *ca.* 20 mJ. Monochromatic probe light was obtained by filtering the output of a 150-W pulsed Xe lamp through two consecutive monochromators, positioned one in front of and the other behind the sample (bandpass 3 and 3 mm).

We thank Prof. *B. Pispisa* (University of Rome, Tor Vergata) for many stimulating discussions. The financial contribution, *MIUR* (PRIN 2006) is also acknowledged.

REFERENCES

[1] H. Duclohier, *Chem. Biodivers.* **2007**, *4*, 1023.
[2] B. Leitgeb, A. Szekeres, L. Manczinger, C. Vagvölgyi, L. Kredics, *Chem. Biodivers.* **2007**, *4*, 1027.
[3] C. Toniolo, E. Benedetti, *Trends Biochem. Sci.* **1991**, *16*, 350.
[4] I. L. Karle, P. Balaram, *Biochemistry* **1990**, *29*, 6747.
[5] Y. Paterson, S. M. Rumsey, E. Benedetti, G. Némethy, A. H. Scheraga, *J. Am. Chem. Soc.* **1981**, *103*, 2947.
[6] L. Zhang, J. Hermans, *J. Am. Chem. Soc.* **1994**, *116*, 11915.
[7] R. Improta, N. Rega, C. Aleman, V. Barone, *Macromolecules* **2001**, *34*, 7550.
[8] C. Toniolo, M. Crisma, F. Formaggio, C. Peggion, *Biopolymers (Pept. Sci.)* **2001**, *60*, 396.
[9] C. Toniolo, M. Crisma, G. M. Bonora, E. Benedetti, B. Di Blasio, V. Pavone, C. Pedone, A. Santini, *Biopolymers* **1991**, *31*, 129.
[10] C. Toniolo, M. Crisma, F. Formaggio, G. Valle, G. Cavicchioni, G. Précigoux, A. Aubry, J. Kamphuis, *Biopolymers* **1993**, *33*, 1061.
[11] C. Toniolo, M. Crisma, F. Formaggio, C. Peggion, Q. B. Broxterman, B. Kaptein, *J. Inclusion Phenom. Macrocyclic Chem.* **2005**, *51*, 121.
[12] L. Stella, G. Bocchinfuso, E. Gatto, C. Mazzuca, M. Venanzi, F. Formaggio, C. Toniolo, A. Palleschi, B. Pispisa, in 'Annual Reviews in Fluorescence', Eds. C. D. Geddes and J. R. Lakowicz, Springer, New York, 2008, in press.
[13] E. Galoppini, M. A. Fox, *J. Am. Chem. Soc.* **1996**, *118*, 2299.
[14] E. Galoppini, M. A. Fox, *J. Am. Chem. Soc.* **1997**, *119*, 5277.
[15] Y.-g. K. Shin, M. D. Newton, S. S. Isied, *J. Am. Chem. Soc.* **2003**, *125*, 3722.
[16] B. Pispisa, 'Chimica Fisica Biologica', 3rd edn., Aracne, Rome, 2007.
[17] T. S. Yokum, T. J. Gauthier, R. P. Hammer, M. L. McLaughlin, *J. Am. Chem. Soc.* **1997**, *119*, 1167.
[18] M. A. Schmitt, S. H. Choi, I. A. Guzei, S. H. Gellman, *J. Am. Chem. Soc.* **2005**, *127*, 13130.
[19] B. Kaptein, W. H. J. Boesten, Q. B. Broxterman, P. J. H. Peters, H. E. Schoemaker, J. Kamphuis, *Tetrahedron: Asymmetry* **1993**, *4*, 1113.
[20] C. L. Wysong, T. S. Yokum, G. A. Morales, R. L. Gundry, M. L. McLaughlin, R. P. Hammer, *J. Org. Chem.* **1996**, *61*, 7650.
[21] M. Amblard, M. Rodriguez, J. Martinez, *Tetrahedron* **1998**, *44*, 5101.
[22] M. T. Leplawy, D. S. Jones, G. W. Kenner, R. C. Sheppard, *Tetrahedron* **1960**, *11*, 39.
[23] A. Moretto, C. Peggion, F. Formaggio, M. Crisma, C. Toniolo, C. Piazza, B. Kaptein, Q. B. Broxterman, I. Ruiz, M. D. Diaz-de-Villegas, J. A. Galvez, C. Cativiela, *J. Pept. Res.* **2000**, *56*, 283.
[24] L. A. Carpino, *J. Am. Chem. Soc.* **1993**, *115*, 4397.
[25] S. L. Murov, I. Carmichael, G. L. Hug, 'Handbook of Photochemistry', Dekker, New York, 1985.
[26] E. W. Thulstrup, P. L. Case, J. Michl, *Chem. Phys.* **1974**, *6*, 410.
[27] S. Y. Kim, G. Y. Lee, S. Y. Han, M. Lee, *Chem. Phys. Lett.* **2000**, *318*, 63.
[28] A. A. Ruth, E.-K. Kim, A. Hese, *Phys. Chem. Chem. Phys.* **1999**, *1*, 5121.
[29] C. Toniolo, A. Polese, F. Formaggio, M. Crisma, J. Kamphuis, *J. Am. Chem. Soc.* **1996,** *118*, 2744.
[30] C. Toniolo, F. Formaggio, S. Tognon, Q. B. Broxterman, B. Kaptein, R. Huang, V. Setnicka, T. A. Keiderling, I. H. McColl, L. D. Barron, *Biopolymers* **2004**, *75*, 32.
[31] R. W. Woody, *Eur. Biophys. J.* **1994**, *23*, 253.
[32] S. Egusa, M. Sisido, Y. Imanishi, *Macromolecules* **1985**, *18*, 882.
[33] S. Mizushima, T. Shimanouchi, M. Tsuboi, R. Souda, *J. Am. Chem. Soc.* **1952**, *74*, 270.
[34] G. M. Bonora, C. Mapelli, C. Toniolo, R. R. Wilkening, E. S. Stevens, *Int. J. Biol. Macromol.* **1984**, *6*, 179.
[35] B. Pispisa, A. Palleschi, L. Stella, M. Venanzi, C. Mazzuca, F. Formaggio, C. Toniolo, Q. B. Broxterman, *J. Phys. Chem., B* **2002**, *106*, 5733.
[36] B. Pispisa, C. Mazzuca, A. Palleschi, L. Stella, M. Venanzi, M. Wakselman, J.-P. Mazaleyrat, M. Rainaldi, F. Formaggio, C. Toniolo, *Chem.–Eur. J.* **2003**, *9*, 4084.
[37] S. L. Murov, I. Carmichael, L. H. Gordon, 'Handbook of Photochemistry', 2nd edn, Dekker, New York, 1993.

[38] J. R. Lakowitz, 'Principle of Fluorescence Spectroscopy', Plenum Press, New York, 1994.
[39] K. D. Kopple, M. Ohnishi, A. Go, *Biochemistry* **1969**, *8*, 4087.
[40] G. P. Zanini, H. A. Montejano, C. M. Previtali, *J. Photochem. Photobiol., A* **2000**, *132*, 161.
[41] Y. Mori, H. Shinoda, T. Nakano, T. Kitagawa, *J. Phys. Chem., A* **2002**, *106*, 11743.
[42] H. A. Montejano, J. J. Cosa, H. A. Garrera, C. M. Previtali, *J. Photochem. Photobiol., A* **1995**, *86*, 115.
[43] C. Borsarelli, H. A. Montejano, J. J. Cosa, C. M. Previtali, *J. Photochem. Photobiol., A* **1995**, *91*, 13.
[44] I. Carmichael, W. P. Helman, G. L. Hug, *J. Phys. Chem. Ref. Data* **1987**, *16*, 239.
[45] P. D. Adams, Y. Chen, K. Ma, M. G. Zagorski, F. D. Sonnichsen, M. L. McLaughlin, M. D. Barkley, *J. Am. Chem. Soc*. **2002**, *124*, 9278.
[46] B. S. Hudson, J. M. Huston, G. Soto-Campos, *J. Phys. Chem., A* **1999**, *103*, 2227.
[47] A. Sillen, *J. Protein Sci.* **2000**, *9*, 158.
[48] B. Donzel, P. Gaudchon, P. Wahl, *J. Am. Chem. Soc*. **1974,** *96*, 801.
[49] A. G. Szabo, D. M. Rayner, *J. Am. Chem. Soc*. **1980**, *102*, 554.
[50] B. D. Wagner, D. T. Helmrich, R. Steer, *J. Phys. Chem*. **1992**, *96*, 7904.
[51] P. A. Muller, E. Vauthey, *J. Phys. Chem., A* **2001**, *105*, 5994.
[52] T. Okada, I. Karaki, N. Mataga, *J. Am. Chem. Soc*. **1982**, *104*, 7191.
[53] R. A. Marcus, N. Sutin, *Biochim. Biophys. Acta* **1985**, *811*, 265.
[54] J. R. Bolton, M. Mataga, G. McLennon, 'Electron Transfer in Inorganic, Organic and Biological Systems', American Chemical Society, Washington, DC, 1991.
[55] E. Gatto, L. Stella, F. Formaggio, C. Toniolo, L. Lorenzelli, M. Venanzi, *J. Pept. Sci.* **2008**, *14*, 184.

Received December 19, 2007